14TH CANADIAN MASONRY SYMPOSIUM
MONTREAL, CANADA
MAY 16TH – MAY 20TH, 2021

MODELING IN-PLANE, OUT-OF-PLANE AND COMBINED FAILURES OF URM STRUCTURES USING A NEW FINITE-DISTINCT MACROELEMENT MODEL

Malomo, Daniele[1] and DeJong, Matthew J.[2]

ABSTRACT

A new Macro-Distinct element model (M-DEM) for the low-cost analysis of both in-plane, out-of-plane and combined failure mechanisms of unreinforced masonry (URM) structures is presented in this work. According to the M-DEM, which is the first macroelement model ever implemented in a discontinuum framework, Finite Element (FE) homogenized macro-blocks are connected by discrete spring interfaces, which accounts for shear/tension damage. Compressive failure, instead, is modeled within the FE macro-blocks, whose layout is determined a priori as a function of the masonry bond pattern. To validate the proposed modeling strategy, previous experimental tests on reduced and full-scale URM specimens are selected and simulated. Both static and dynamic loading protocols are considered, as well as a variety of different masonry types, boundary conditions, vertical surcharges, and confinement levels. The results indicate that the M-DEM can satisfactorily reproduce the behavior of in-plane and out-of-plane-loaded URM components, as well as their response under combined actions, in a reasonable timeframe, in terms of both force-displacement relationship, dissipated energy and failure modes.

KEYWORDS: *discrete element method, finite element method, macroelement, in-plane, out-of-plane, unreinforced masonry*

[1] Assistant Professor, Department of Civil Engineering and Applied Mechanics, McGill University, 817 Sherbrooke Street, Montréal, QC, Canada, daniele.malomo@mcgill.ca

[2] Associate Professor, Department of Civil and Environmental Engineering, University of California, Berkeley, 777 Davis Hall, Berkeley, California, United States, dejong@berkeley.edu

INTRODUCTION

Simplified macro-models often represent the preferred choice for the low-cost modeling in-plane (IP) governed responses of both reduced and large-scale unreinforced masonry (URM) structures [1,2]. Amongst others, Equivalent-frame (EFM) modeling strategies e.g. [3,4], according to which a given URM system is typically idealized as an assembly of spandrel, pier and rigid node elements, are widely employed by both practitioners and researchers, and endorsed by many international codes. However, in the presence of irregular opening layouts, the identification of the effective height/length of URM members becomes non-unique and may lead to epistemic modeling errors [5], resulting in a significant dependency of predicted results on the considered discretization scheme [6]. Further, notwithstanding the possibility of obtaining unconservative predictions, the effects of out-of-plane (OOP) failures, as well as the mechanical interaction among elements subjected to IP-OOP combined actions, are typically neglected. Although promising novel modeling strategies are currently being explored [7,8], the low-cost numerical assessment of OOP-governed responses and the simulation of IP-OOP combined failures of URM structures still represents an open challenge. On the other hand, the applications of more complex micro-modeling strategies, based on e.g. Finite [9] and Distinct (or Discrete) [10] Element techniques to the numerical simulation of large-scale URM systems, is often computationally unfeasible.

In this work, to combine the efficiency of simplified approaches with the multifaceted capabilities of interface-based discontinuum methods, a new Macro-Distinct Element Model (M-DEM) for the analysis of URM structures is presented and validated against a wide range of laboratory tests on both reduced and full-scale brick and block URM prototypes subjected to IP, OOP and combined IP-OOP actions and tested under either static or dynamic loading, different boundary conditions, vertical surcharges, and confinement levels. The novel approach is implemented within the 3DEC Distinct Element Method commercial software [11] and might be of interest to both practitioners and researchers. Further, the explicit time-integration scheme on which the selected computational platform is founded makes this model compatible with large-displacement and collapse analysis.

M-DEM MODELING STRATEGY FOR URM STRUCTURES

In the framework of M-DEM, each URM member is idealized an assembly of six deformable FE macro-blocks (see Figure 1(a)), characterized by an internal tetrahedral mesh, connected to each other by means of horizontal, vertical and diagonal nonlinear spring layers, whose number and layout is determined *a priori* as a function of aspect ratio λ_w (calculated as h_w/l_w, i.e. wall height over its length, see Figure 1(b)) and masonry texture of the considered URM component.

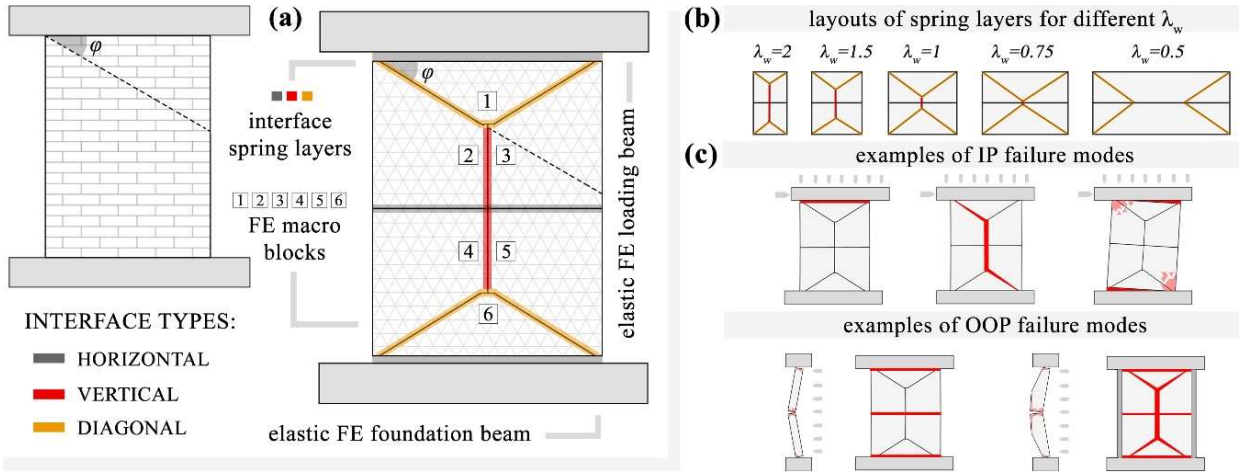

Figure 1: (a) M-DEM idealization, (b) spring layers layout as a function of the aspect ratio, (c) examples of IP/OOP failures

The average slope (φ) of the lines connecting consecutive head joints along the height/length of a given masonry element [12], is used to define potential failure planes for the development of discrete cracks between the FE blocks. Such a simplified discretization scheme, as exhaustively discussed in [13], has been conceived in order to reproduce the main failure modes typically observed during experimental IP tests on both URM spandrels and URM wall components [14,15] – without the need of assuming the effective height of piers, which is one of the main limitation of EFM models. Meanwhile, as qualitatively shown in Figure 1(c) and demonstrated in [16], it also enables the possibility of simulating the main OOP collapse modes under both one-way [17] and two-way [18] bending. Shear and tensile failures are accounted for by the interface springs, characterized by a Mohr-Coulomb criterion (no shear softening) with tension cut-off and to which normal (k_n) and tangential (k_s) dummy stiffnesses are assigned (see Figure 2(a)). While friction angle ϕ, cohesion c and tensile strength f_t of horizontal joints are assumed equal to those inferred through triplet and bond wrench tests respectively, equivalent values (i.e. $\bar{\phi}, \bar{c}, \bar{f}_t$) are calculated for the diagonal joints as a function of φ, using Equations (1), (2), (3).

$$\bar{\phi} = \frac{\phi\cos(\varphi) + \sin(\varphi)}{\cos(\varphi) - \phi\sin(\varphi)} \tag{1}$$

$$\bar{c} = \frac{c\cos(\varphi)}{\cos(\varphi) - \phi\sin(\varphi)} \tag{2}$$

$$\bar{f}_t = \frac{f_t}{\cos(\varphi)} \tag{3}$$

On the other hand, the equivalent shear/tensile strength parameter (i.e. $\bar{\bar{c}} = \bar{\bar{f}}_t$, Equation (4)) proposed by Beyer [19], evaluated also considering the resistance provided by interlocking units (with thickness t_u, length l_u and width w_u), is specified for the t_j-thick vertical joints.

$$\bar{\bar{c}} = \bar{\bar{f}}_t = \frac{c\left(t_u + t_j\right) + \left(l_u \phi\right)\left(\phi + c\right)/1.5}{2\phi\left(t_u + t_j\right)} \tag{4}$$

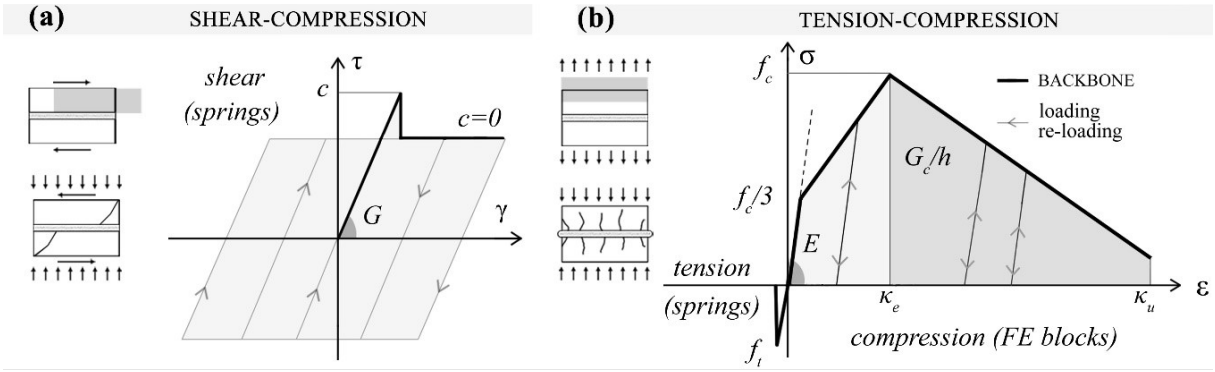

Figure 2: (a) Tension-compression and (b) shear-compression M-DEM constitutive laws

A linearized version of the Feenstra-De Borst strain-softening compression model [20] (see Figure 2 (b)), initially conceived for simulating concrete failure, was implemented in 3DEC and assigned to the FE blocks to account for masonry crushing. This represents the first attempt to include a FE blocks compressive failure criterion in the 3DEC environment. As shown in [13], and despite the differences between clay brick and concrete materials, satisfactory results can be obtained simulating either small, reduce or full-scale URM assemblies.

COMPARISON AGAINST EXPERIMENTAL IN-PLANE CYCLIC TESTS

Two reduced-scale double-wythe (English bond pattern, $\varphi \simeq 28$) clay brick masonry walls, hereinafter referred to as LW (i.e. i.e. squat low-wall, 0.25x1x1m) and HW (i.e. slender high-wall, 0.25x1.35x2m), were tested under fixed-fixed boundary conditions and quasi-static in-plane cyclic loading at the Joint Research Center (Ispra, Italy) by Anthoine et al. [21]. A constant vertical overburden stress of 0.6 MPa was applied to both walls. The experimental mechanical properties are reported in Table 1 together with those inferred analytically using the Equations (1)-(4), where G_c is fracture energy in compression and G_m stands for masonry shear modulus (derived assuming material isotropy, i.e. G_m =0.4E_m).

Table 1: Experimental IP material properties and equivalent M-DEM parameters

E_m	G_m	k_n	k_s	f_c	f_t	c	$\bar{f}_t$	$\bar{c}$	$\bar{\bar{c}}$	ϕ	φ	$\bar{\phi}$	G_c
MPa	MPa	MPa/m	MPa/m	MPa	MPa	MPa	MPa	MPa	MPa	°	°	°	N/mm
1491	596	14.9	5.9	6.2	0.6	0.2	0.7	0.3	1.3	30	28	58	1.0

In Figure 3, numerical results for different FE mesh sizes, characterized by a maximum element length (EL) values of 0.05, 0.10 and 0.20m, are compared with their experimental counterparts. For both LW and HW, the overall hysteretic response has been adequately captured by the M-DEMs; acceptable agreement between experimental and numerical (absolute) peak base shear and initial stiffness was found, with only slight differences for different FE mesh sizes. Similarly, total energy dissipation and ultimate displacement capacities (determined numerically as the displacement at which the panel is no longer able to carry vertical load) generally compared well. However, for HW models, measured dissipated energy was noticeably underestimated. Similar issues were also experienced by other researchers using either macro [22] and micro [23] models.

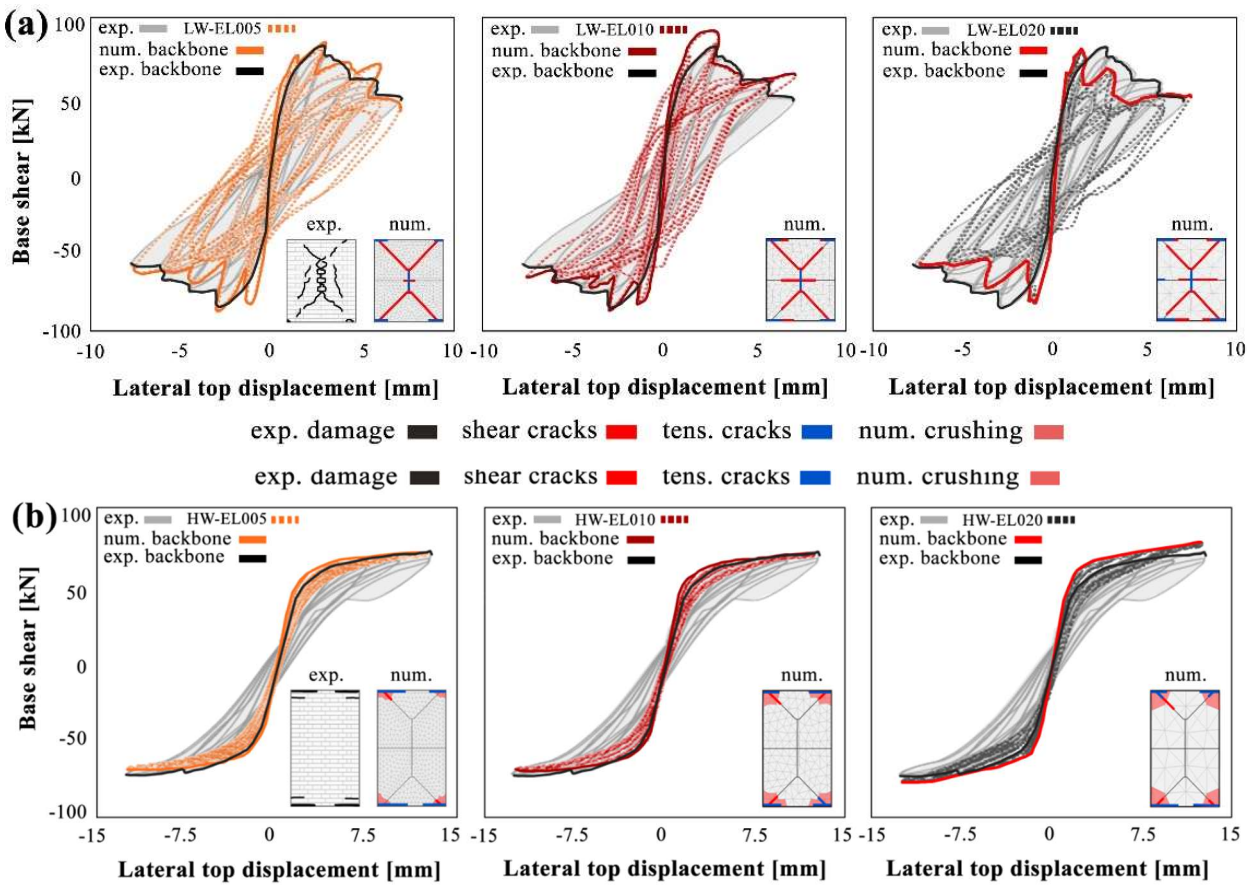

Figure 3: Exp. vs num. hysteretic response and crack pattern of (a) LW and (b) HW

In what follows, to extend the methodology presented and validated above to building-scale structures, a two-story URM façade (0.25x4.4x6.4m, see Figure 4(a)) with flexible diaphragms (to which increasing horizontal forces and constant vertical surcharge of 0.01MPa/floor were applied) tested at the University of Pavia in 1995 [24] under quasi-static IP cyclic loading (Figure 4(b)), was modeled. Being part of the same experimental campaign of LW/HW, same assumptions and material properties were also adopted for the modeling of the façade (herein named DW, i.e. door-wall). As shown in Figure 4(c), except for the diagonal cracks of the 2nd floor central pier, both the simulated damage and hysteretic curve show adequate agreement with test data. Interested readers

may refer to [13], where the qualitative observations above are supported by the ratio among predicted and measured key quantities for each of the considered tests and models.

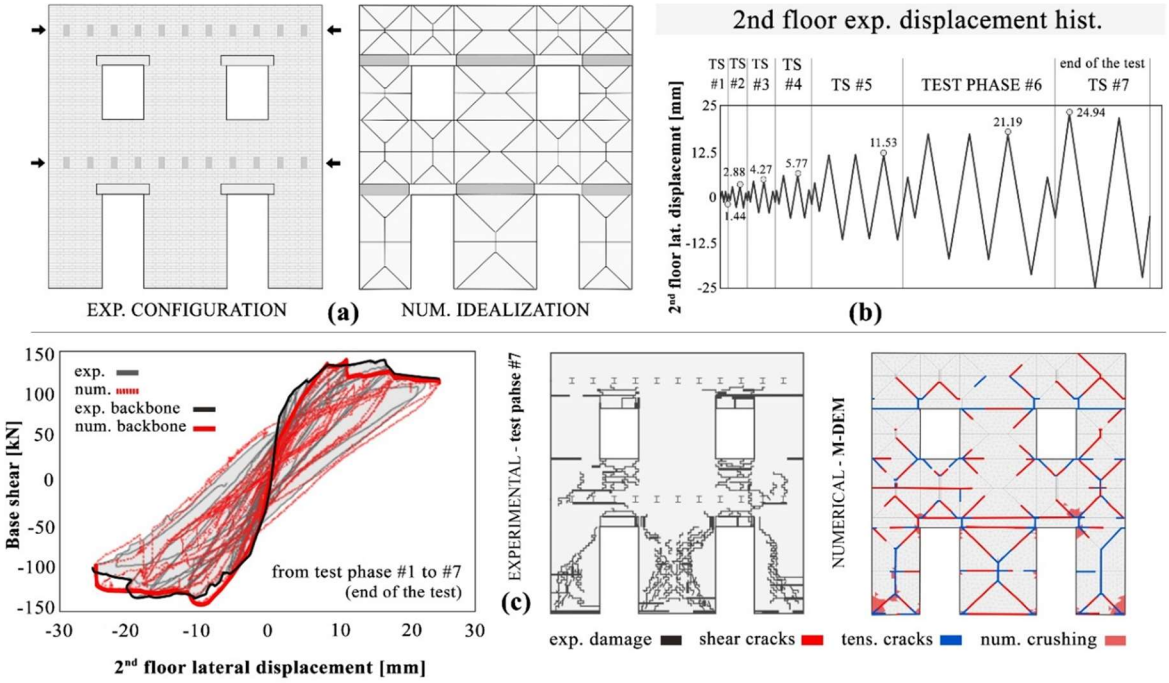

Figure 4: (a) Exp. configuration and num. idealization, (b) 2nd floor experimental displacement history, (c) exp. vs num. hysteretic response and crack pattern

VALIDATION WITH ONE AND TWO-WAY OUT-OF-PLANE MONOTONIC TESTS

In this section, the outcomes of a various OOP monotonic air-bag tests on URM walls, subjected to either one-way (1WB) or two-way (2WB) bending until failure, are compared in this section with M-DEM predictions.

1WB tests are those conducted by [25], and include both solid clay brick (i.e. specimens 6-3 and 6-7, 0.09x1.25x2.44m) and a concrete block walls (i.e. specimen 3-3, 0.19x1.21x2.44m). Relatively high vertical top loads (5.41, 11.20 and 0.47 MPa, assigned to walls 6-3, 6-7 and 3-3 respectively) were imposed through a steel beam, resulting in a crushing-dominated response. With reference to the 2WB specimens, the first two panels are identical reduced-scale clay brick prototypes (specimens 8 and 12, 0.053x0.79x1.19 x m) tested at the University of Edinburgh, Scotland [26]. Both specimens exhibited an hourglass-shaped crack pattern, where mid-height central bricks and those in contact with the fixed external frame also failed in compression. The remaining prototype is a concrete block URM wall (named WI, 0.15x4x2.8m) tested at McMaster University, Canada [27]. In this case, mortar joint failure was predominant, although minor damage due to compressive stress localizations was observed at mid-height.

Analogous assumptions to that of the models of the previous section; adopted material properties are summarized in Table 2 below:

Table 2: Experimental OOP material properties and equivalent M-DEM parameters

Wall ID	E_m MPa	G_m MPa	k_n MPa/m	k_s MPa/m	f_c MPa	f_t MPa	c MPa	$\bar{f}_t$ MPa	$\bar{c}$ MPa	$\bar{\bar{c}}$ MPa	ϕ °	φ °	$\bar{\phi}$ °	G_c N/mm
3-3	6206	2482	62.1	24.8	11.4	0.2	0.1	0.2	0.9	0.5	44.3	30	74.4	19.4
6-3	20685	8274	206.9	82.7	50.5	1.5	0.8	2.1	2.4	2.5	29.3	30	59.4	27.5
6-7	20685	8274	206.9	82.7	50.5	1.5	0.8	2.1	2.4	2.5	29.3	30	59.4	27.5
8/12	15000	6000	150.0	60.0	6.0	0.1	0.2	0.2	0.4	0.8	33.1	30	65.8	17.4
WI	10000	4000	100.0	40.0	20.0	0.3	0.4	0.3	1.6	1.0	44.2	30	74.1	22.2

Experimental and numerical results are compared in Figure 5 in terms of OOP force-displacement curves. In the case of the specimens 3-3 and 6-7, the local crushing failure modes was adequately captured, although the ultimate displacement capacities were noticeably overestimated. Better agreement in this sense was found for 6-3, which mainly suffered mortar joint failures.

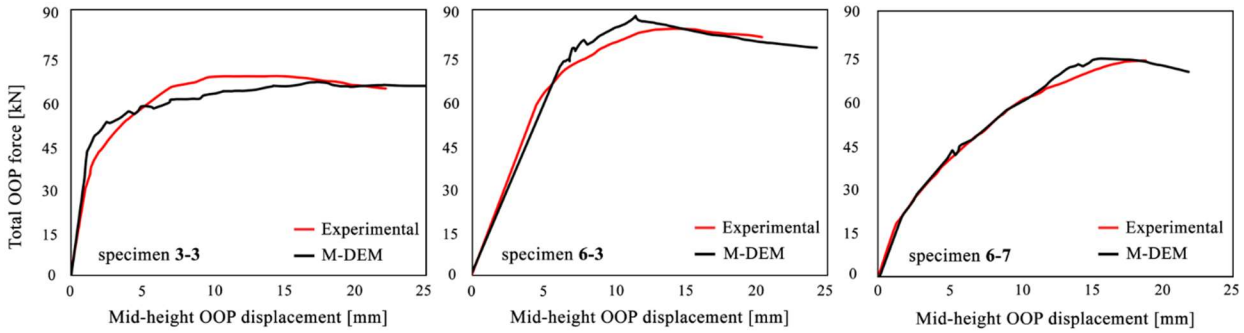

Figure 5: 1WB: exp. vs. num OOP force-displacement curves

As shown in Figure 5, the OOP response of wall 8/12 predicted by the M-DEM model is in good agreement with the experimental results, for both force-displacement curves and failure modes, also considering the variability between the two identical experimental tests. The numerically-inferred peak OOP force is closer to the wall 12 result and agrees well with the prediction by [28] who employed a more detail FEM-based interface meso-model.

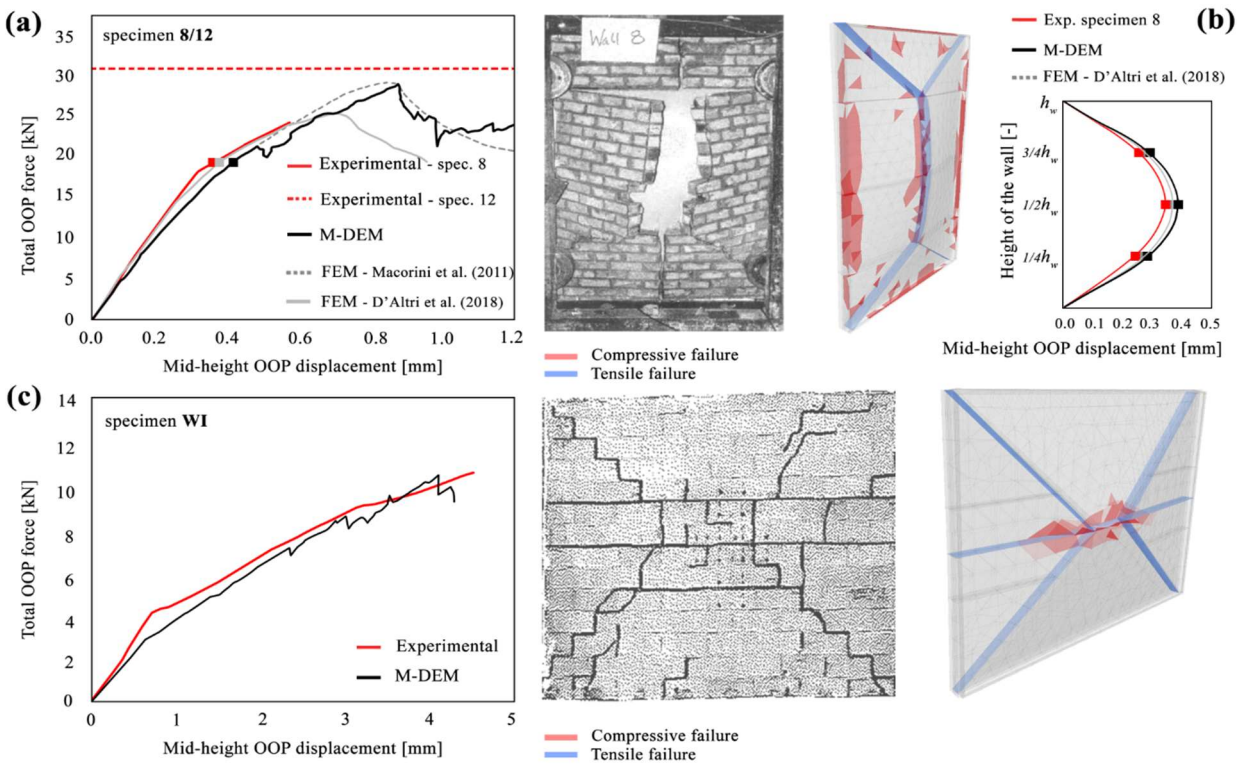

Figure 6: 2WB: exp. vs. num (a) OOP force-displacement curves, failure modes and (b) displacement profiles for specimens 8/12 and (c) WI respectively

SIMULATING COMBINED IP-OOP FAILURE MODES

Given the satisfactory results obtained for both IP and OOP-loaded URM assemblies, the M-DEM modeling strategy is applied in this section to the simulation of the dynamic response of a full-scale double-wythe clay brick U-shaped specimen (see Figure 7; front façade 0.23x3.5x2.25m, return walls 0.23x2.5x2.25m), for which IP-OOP interaction played a relevant role. The specimen has been tested up to collapse on the shake-table of the LNEC laboratory (Lisbon, Portugal) in 2014, under incremental loading protocol [29] (from TEST01 – peak ground acceleration, PGA=0.18g, to TEST08 – PGA=1.27g; neither top restraints nor vertical surcharge were imposed).

The material properties implemented in the M-DEM model are summarized in Table 3 below:

Table 3: Experimental IP-OOP material properties and equivalent M-DEM parameters

E_m	G_m	k_n	k_s	f_c	f_t	c	$\bar{f}_t$	$\bar{c}$	$\bar{\bar{c}}$	ϕ	φ	$\bar{\phi}$	G_c
MPa	MPa	MPa/m	MPa/m	MPa	MPa	MPa	MPa	MPa	MPa	°	°	°	N/mm
5170	2068	51.7	20.68	25.0	0.1	0.2	0.1	0.4	0.8	36.9	35	71.9	23.5

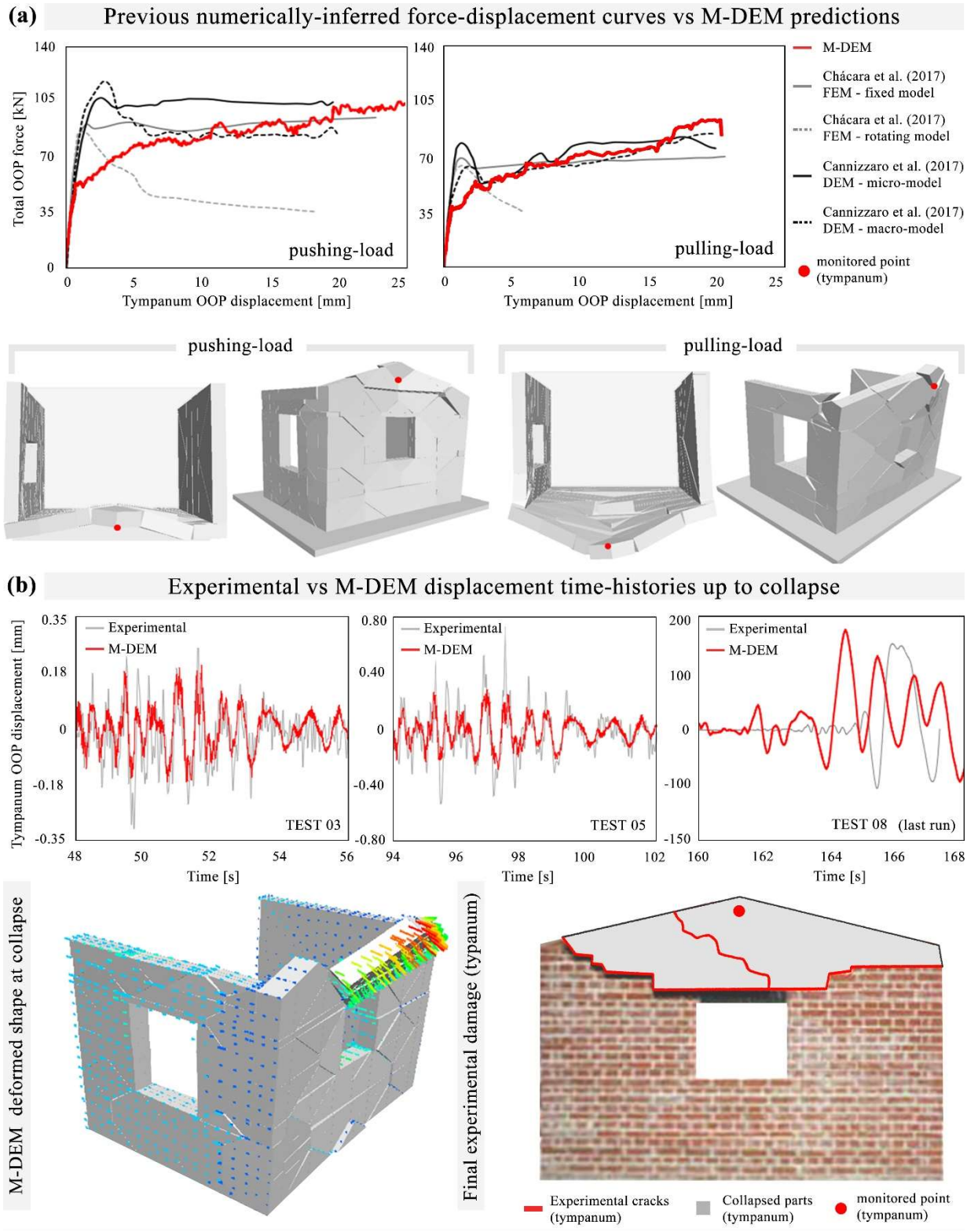

Figure 7: 2WB: (a) M-DEM IP-OOP monotonic force-displacement curves and failure modes vs previous num. results, failure modes, (b) exp. vs M-DEM outcomes

To validate the proposed M-DEM model with respect to combined IP-OOP actions, two different modeling exercises have been conducted. First, quasi-static monotonic analyses were performed applying a uniform pressure to the front façade (both pushing and pulling loads were considered), and the associated results compared to those obtained by other authors using FEM ([30], both rotating and fixed crack models were employed) and DEM [31] models. As depicted in Figure 7(a), the force-displacement curves predicted by the M-DEM are comparable to the selected FEM/DEM counterparts, even though the peak base shear was reached at considerably higher deformation levels. Acceptable agreement was also found in terms of simulated damage of both front façade and return walls.

Finally, the shake-table incremental loading protocol was considered, and the M-DEM outcomes were compared to the experimental ones. For this model, 5% mass-proportional damping acting at a critical frequency of 21Hz was employed. From Figure 7(b), where measured and numerical displacement time-histories are plotted against each other for selected test phases only due to space constraints, it can be gathered that the M-DEM was capable of reproducing the experimentally-observed dynamic response at markedly different damage levels, from the uncracked state (i.e. TEST03), to the partial collapse of the tympanum (i.e. TEST08, after which the test was stopped).

It is worth noting that the collapse mechanism was explicitly reproduced by the M-DEM, and that, despite minor differences with respect to peak displacements (possibly due to impact phenomena during the test, which may be captured numerically using zero damping – this aspect is currently being investigated), the recorded signals are in phase and deformation magnitudes comparable.

CONCLUSIONS

Simplified macro-models are widely employed by both practitioners and researchers, representing an acceptable compromise between accuracy and analysis time. However, their applicability is often limited to IP-governed responses of URM structures with regular opening layouts. On the other hand, although advanced micro-modeling techniques are naturally suitable for modeling complex geometries and simulating OOP failure modes, analyzing of large-scale URM structures is presently computationally unfeasible.

To overcome the abovementioned limitations, a novel Macro-Distinct element model (M-DEM) that combines the efficiency of simplified approaches with the multifaceted capabilities of interface-based discontinuum methods, is presented and validated in this work. Unlike previous macro-models, the M-DEM is capable of simulating IP, OOP and combined IP-OOP mechanisms, with adequate accuracy and in a reasonable timeframe. Indeed, despite minor differences observed in some simulations, the quasi-static IP cyclic interaction between stiffness degradation and energy dissipation rate was satisfactorily accounted for numerically. Similarly, an acceptable agreement was found when comparing measured and predicted OOP monotonic force-displacement curves and associated damage, due to either one-way or two-way bending. Finally, taking advantage from the previous modeling exercises, the experimentally-observed impact of combined IP-OOP actions on the shake-table response of a full-scale URM U-shaped prototype was reproduced using the M-

DEM, up to partial collapse. This last aspect constitutes a major achievement because most of the presently-available macro-models are not capable of modeling structural behaviors beyond near-collapse conditions. Comparable outcomes were obtained in terms of both predicted displacement magnitudes (monitored at the tympanum level) and overall damage pattern.

Given the adequate results obtained and the relatively low computational cost, the proposed methodology would represent a valid alternative to more detailed analysis techniques, which might be also considered for supporting seismic risk assessment investigations of large-scale URM structures and building aggregates under dynamic loading. The latter, amongst others, is one of the research directions currently being explored.

ACKNOWLEDGEMENTS

Prof. Guido Magenes, Prof. Andrea Penna (University of Pavia, Italy), Prof. Paulo Lourenço (University of Minho, Portugal) and Dr. Antonio Maria D'Altri (University of Bologna, Italy) are gratefully acknowledged for their precious assistance in accessing experimental and numerical data used in this manuscript for comparison purposes.

REFERENCES

[1] Sangirardi M., Liberatore D., Addessi D. (2019). Equivalent Frame modelling of masonry walls based on plasticity and damage. *Int J Archit Herit*, 13:1098–109.

[2] Kallioras S., Graziotti F., Penna A. (2019). Numerical assessment of the dynamic response of a URM terraced house exposed to induced seismicity. *Bull Earthq Eng*, 17:1521–52.

[3] Lagomarsino S., Penna A., Galasco A., Cattari S. (2013). TREMURI program: an equivalent frame model for the nonlinear seismic analysis of masonry buildings. *Eng Struct*, 56:1787.

[4] Raka E., Spacone E., Sepe V., Camata G. (2015). Advanced frame element for seismic analysis of masonry structures: model formulation and validation. *Earthq Eng Struct Dyn,* 44:2489–506.

[5] Berti M., Salvatori L., Orlando M., Spinelli P. (2017). Unreinforced masonry walls with irregular opening layouts: reliability of equivalent-frame modelling for seismic vulnerability assessment. *Bull Earthq Eng*, 15:1213–39.

[6] Quagliarini E., Maracchini G., Clementi F. (2017). Uses and limits of the Equivalent Frame model on existing unreinforced masonry buildings for assessing their seismic risk: A review. *J Build Eng*,10:166–82.

[7] Vanin F., Penna A., Beyer K. (2020). A three-dimensional macroelement for modelling the in-plane and out-of-plane response of masonry walls. *Earthq Eng Struct Dyn* - in press.

[8] Pantò B., Cannizzaro F., Caliò I., Lourenço P. (2017) Numerical and experimental validation of a 3D macro-model for the in-plane and out-of-plane behavior of unreinforced masonry walls. *Int J Archit Herit*, 11:946–64.

[9] D'Altri A.M., de Miranda S., Castellazzi G., Sarhosis V. (2018). A 3D detailed micro-model for the in-plane and out-of-plane numerical analysis of masonry panels. *Comput Struct,* 206:18–30.

[10] Malomo D., DeJong M.J., Penna A. (2019). Distinct element modelling of the in-plane cyclic response of URM walls subjected to shear-compression. *Earthq Eng Struct Dyn*, 48:1322–44.

[11] Itasca Consulting Group Inc. 3DEC. (2013) Three dimensional Distinct Element code.

[12] Malomo D., DeJong M.J., Penna A. (2019). Influence of bond pattern on the in-plane behavior

of URM piers. *Int J Archit Herit* - in press.
[13] Malomo D., DeJong M.J. (2020). A Macro-Distinct Element Model (M-DEM) for simulating the in-plane cyclic behavior of URM structures. *Eng Struct*, 227:111428.
[14] Magenes G., Calvi G.M. (1997). In-plane seismic response of brick masonry walls. *Earthq Eng Struct Dyn*, 26:1091–112.
[15] Beyer K., Dazio A. (2021). Quasi-static cyclic tests on masonry spandrels. *Earthq Spectra*, 28:907–29.
[16] Malomo D., DeJong M.J. (2021). A Macro-Distinct Element Model (M-DEM) for out-of-plane analysis of unreinforced masonry structures. *Eng Struct* - under review.
[17] Penner O., Elwood K.J. (2016). Out-of-plane dynamic stability of unreinforced masonry walls in one-way bending: Shake table testing. *Earthq Spectra*, 32:1675–97.
[18] Griffith M.C., Vaculik J., Lam N.T.K., Wilson J., Lumantarna E. (2007). Cyclic testing of unreinforced masonry walls in two-way bending. *Earthq Eng Struct Dyn*, 36:801–21.
[19] Beyer K. (2012). Peak and residual strengths of brick masonry spandrels. *Eng Struct,* 41:533.
[20] Feenstra P.H., De Borst R. (1996). A composite plasticity model for concrete. *Int J Solids Struct*, 33:707–30.
[21] Anthoine A., Magonette G., Magenes G. (1995). Shear-compression testing and analysis of brick masonry walls. *Proc. 10th Eur. Conf. Earthq. Eng.*, Rotterdam, The Netherlands.
[22] Penna A., Lagomarsino S., Galasco A. (2014). A nonlinear macroelement model for the seismic analysis of masonry buildings. *Earthq Eng Struct Dyn*, 43:159–79.
[23] Malomo D., Pinho R., Penna A. (2018). Using the applied element method for modelling calcium silicate brick masonry subjected to in-plane cyclic loading. *Earthq Eng Struct Dyn*, 47:1610–30.
[24] Magenes G., Kingsley G.R., Calvi G.M. (1995). Seismic Testing of a full-Scale, two-story masonry building : test procedure and measured experimental response. *CNR technical report* [in Italian].
[25] Yokel F.Y., Mathey R.G., Dikkers R.D. (1971). Strength of masonry walls under compressive and transverse loads. *Dept Commer United States technical report*.
[26] Chee Liang N. (1996). Experimental and theoretical investigation of the behaviour of brickwork cladding panel subjected to lateral loading. *PhD Dissertation* - Dept Civ Environ Eng Univ Edinburgh, Scotland.
[27] Drysdale R.G., Essawy A.S. (1988). Out-of-plane bending of concrete block walls. *J Struct Eng*, 114:121–33.
[28] Macorini L., Izzuddin B.A. (2011). A non-linear interface element for 3D mesoscale analysis of brick-masonry structures. *Int J Numer Methods Eng,* 85:1584–608.
[29] Candeias P.X., Campos Costa A., Mendes N., Costa A.A., Lourenço P. (2017). Experimental assessment of the out-of-plane performance of masonry buildings through shaking table tests. *Int J Archit Herit*, 11:125–42.
[30] Chácara C., Mendes N., Lourenço P. (2017). Simulation of shake table tests on out-of-plane masonry buildings. Part (IV): macro and micro FEM based approaches. *Int J Archit Herit,* 11:103–16.
[31] Cannizzaro F., Lourenço P. (2017). Simulation of shake table tests on out-of-plane masonry buildings. Part (VI): Discrete Element approach. *Int J Archit Herit,* 11:125–42.